Elsevier Editorial System(tm) for Computer Methods in Applied Mechanics and Engineering

Manuscript Draft

Manuscript Number:

Title: A Finite Element Method for Simulating Fluid Motion in Librating Triaxial Ellipsoids: Numerical Theory and Application

Article Type: Research Paper

Keywords: planetary libration, triaxial ellipsoid, finite element method

Corresponding Author: Professor Keke Zhang, PhD

Corresponding Author's Institution: University of Exeter

First Author: Keke Zhang, PhD

Order of Authors: Keke Zhang, PhD; Kit Chan, PhD; Yinnian He, PhD; Jun Zou, PhD

Abstract:
Fluid motion driven by planetary libration may play a key role in
maintaining the magnetism of synchronous planets
and moons that are thermally or chemically non-convective.
We present an efficient finite element method, based on
the three-dimensional triangulation of a triaxial ellipsoidal domain with
the velocity and pressure being represented by continuous
piecewise quadratic and linear finite elements,
for simulating nonlinear flows in latitudinally librating, triaxial ellipsoidal cavities.
Stability properties of the time-dependent finite element solution are studied and
errors of the finite element solution are estimated.
Two different temporal schemes with
the same spatial tetrahedral discretization are implemented for
a librating triaxial ellipsoid,
offering an insight into the practical aspect of the proposed finite element scheme.

Suggested Reviewers: Ping Lin PhD
Professor , Department of Mathematics, University of Dundee
plin@maths.dundee.ac.uk

Dr. Lin is an expert on this subject of research.

Opposed Reviewers:

Highlights: A Finite Element Method for Simulating Fluid Motion in Librating Triaxial Ellipsoids: Numerical Theory and Application

Kit H. Chan [a], Yinnian He [b], Keke Zhang [c,1] and Jun Zou [d]

[a] *Department of Mathematics, The University of Hong Kong, Pokfulam, Hong Kong*

[b] *Center for Computational Geosciences, School of Mathematics and Statistics, Xi'an Jiaotong University, China*

[c] *Department of Mathematical Sciences, University of Exeter, EX4 4QF, UK, and the Institute of Mathematical Sciences, Chinese University of Hong Kong, Shatin, Hong Kong*

[d] *Department of Mathematics, The Chinese University of Hong Kong, Shatin, Hong Kong*

---

(1) Fluid motion driven by planetary libration may maintain the magnetism of synchronous planets;

(2) An efficient finite element method is presented for simulating nonlinear flows in librating triaxial ellipsoidal cavities;

(3) Stability properties of the time-dependent finite element solution are analyzed;

(4) Errors of the finite element solution are estimated;

(5) Two different temporal schemes are implemented for a librating triaxial ellipsoid.

[1] Corresponding author. E-mail address: kzhang@ex.ac.uk

A Finite Element Method for Simulating Fluid Motion in Librating Triaxial Ellipsoids: Numerical Theory and Application

Kit H. Chan [a], Yinnian He [b], Keke Zhang [c,1] and Jun Zou [d]

[a] *Department of Mathematics, The University of Hong Kong, Pokfulam, Hong Kong*

[b] *Center for Computational Geosciences, School of Mathematics and Statistics, Xi'an Jiaotong University, China*

[c] *Department of Mathematical Sciences, University of Exeter, EX4 4QF, UK, and the Institute of Mathematical Sciences, Chinese University of Hong Kong, Shatin, Hong Kong*

[d] *Department of Mathematics, The Chinese University of Hong Kong, Shatin, Hong Kong*

Abstract

Fluid motion driven by planetary libration may play a key role in maintaining the magnetism of synchronous planets and moons that are thermally or chemically non-convective. We present an efficient finite element method, based on the three-dimensional triangulation of a triaxial ellipsoidal domain with the velocity and pressure being represented by continuous piecewise quadratic and linear finite elements, for simulating nonlinear flows in latitudinally librating, triaxial ellipsoidal cavities. Stability properties of the time-dependent finite element solution are studied and errors of the finite element solution are estimated. Two different temporal schemes with the same spatial tetrahedral discretization are implemented for a librating triaxial ellipsoid, offering an insight into the practical aspect of the proposed finite element scheme.

Key words: Finite Element Method, Numerical Stability, Triaxial Ellipsoids

[1] Corresponding author. E-mail address: kzhang@ex.ac.uk

1 INTRODUCTION

The shape of many planets and moons is, to a first approximation, spherical. It is well known, however, that, because of the rapid rotation of planets and moons as well as the interaction among the Sun, planets and moons, many astrophysical bodies are non-spherical and in the shape of a spheroid or a triaxial ellipsoid [16]. As a result of non-spherical geometry, planets and moons are usually rotating non-uniformly and undergo forced libration [18]. It is recently revealed, through an asymptotic theory [24], that fluid motion in a synchronously rotating spheroidal planet can resonate with planetary latitudinal libration, leading to a large amplitude $\mathrm{O}(E^{-1/2})$ of the librationally driven flow, where the Ekman number E is extremely small for many rapidly rotating planets. It suggests an alternative driving mechanism for the dynamo action of planets and moons that are thermally or chemically non-convective. The libration-driven mechanism is feasible because the two conditions for resonance – nearly synchronous rotation and small but non-zero eccentricity of the shape – can be approximately met by many synchronous planets and moons.

In comparison with spherical geometry, direct numerical simulation in triaxial ellipsoidal geometry is mathematically and computationally less tractable. Although ellipsoidal geometry can be, in principle, accommodated by a coordinate transformation that maps an ellipsoidal domain into the spherical domain [17] or by complicated non-spherical coordinates [20], there are computational disadvantages in the pseudo-spectral approximation with the poloidal-toroidal decomposition and, particularly, the mathematical equations resulting from the coordinate transformation are highly complicated. Moreover, the harmonic expansion must lead to the global integration that requires an intensive global communication, making it less efficient on modern massively parallel computers. It is hence desirable to seek an alternative numerical method that is non-spectral and can be readily implemented on modern parallel computers for solving the problem of fluid mechanics in librating triaxial ellipsoids.

The present study concerns with a finite element method suitable for simulating the nonlinear flow of a homogeneous fluid of viscosity ν driven by latitudinal libration and confined within a triaxial ellipsoidal cavity. The triaxial ellipsoidal cavity of arbitrary eccentricity $\mathcal{E}$ is described by

$$\frac{x^2}{a^2} + \frac{y^2}{a^2(1+\mathcal{E}^2)} + \frac{z^2}{a^2(1-\mathcal{E}^2)} = 1, \tag{1}$$

where $0 < \mathcal{E} < 1$, which also defines Cartesian coordinates (x, y, z) used in the numerical analysis. The ellipsoidal container rotates rapidly with an angular velocity $\mathbf{\Omega}_0$ fixed in an inertial frame and, at the same time, undergoes weak latitudinal libration with the libration vector $\mathbf{\Omega}_{lat}$ which results in a periodic variation of the z-axis of the ellipsoid towards and away from its mean direc-

tion. Through both viscous and topographic coupling between the container and the interior fluid, latitudinal libration can drive fluid motion against viscous dissipation. There are three key parameters that characterize the problem of librationally driven flow in triaxial ellipsoidal cavities: the Ekman number $E = \nu/(a^2\Omega_0)$, where $\Omega_0 = |\mathbf{\Omega}_0|$, provides the measure of relative importance between the typical viscous force and the Coriolis force, the eccentricity $\mathcal{E}$ measures the degree of topographic coupling between the container and its interior fluid, and the Poincaré number Po quantifies the strength of Poincaré force resulting from the libration. All these three parameters are believed to be small for a typical planet and, hence, we shall focus on the case with $Po \ll 1$ and $E \ll 1$.

For simulating fluid motion driven by latitudinal libration in triaxial ellipsoids, we shall employ an EBE (Element-By-Element) finite element method that has been effectively used for the numerical solution of the dynamo problem in spherical geometry [1,2]. While the practical aspects of the finite element method, such as how to perform temporal discretization and spatial tetrahedral discretization, have been discussed, its key theoretical properties, particularly the numerical stability of the finite element scheme and the numerical error of the finite element solution, have not been studied for librationally driven flows in triaxial ellipsoidal geometry. Such theoretical studies will be essential for the geophysical and astrophysical application of the numerical method. The primary purpose of this paper is to understand the theoretical aspects of the finite element method – which is based on the three-dimensional triangulation of the triaxial domain together with the velocity and pressure being represented by continuous piecewise quadratic and linear finite elements – for simulating a nonlinear flow in latitudinally librating triaxial ellipsoids. By providing the mathematical analysis on the numerical stabilities and error estimates, we build a mathematically sound framework for numerically simulating a nonlinear flow in latitudinally librating triaxial ellipsoids.

In what follows we shall begin by presenting the model and governing equations of the numerical problem in Section 2. The theoretical problem of the finite element method is discussed in Section 3 and Section 4. Numerical results are presented in Section 5 and the paper closes in Section 6 with a brief summary and concluding remarks.

2 MODEL AND GOVERNING EQUATIONS

Consider a homogeneous fluid of viscosity ν confined within a triaxial ellipsoidal cavity defined by (1). Suppose that the ellipsoidal container rotates rapidly with an angular velocity $\mathbf{\Omega}_0$ which is fixed in the inertial frame and, at the same time, undergoes latitudinal libration with the libration vector $\mathbf{\Omega}_{lat}$

which results in a periodic variation of the z-axis slightly towards and away from the rotation axis $\mathbf{\Omega}_0$. Motivated by its application to synchronous planets and moons, we assume that the overall angular velocity, $\mathbf{\Omega} = \mathbf{\Omega}_0 + \mathbf{\Omega}_{lat}$, of the triaxial ellipsoidal container can be expressed as

$$\mathbf{\Omega} = \mathbf{\Omega}_0 + \hat{\mathbf{x}}\Omega_0 Po \sin(\hat{\omega}\Omega_0 t), \tag{2}$$

where $\hat{\mathbf{x}}$ is a unit vector that is fixed in a frame of reference attached to the container, the mantle frame of reference, and perpendicular to the angular velocity $\mathbf{\Omega_0}$, and $Po/\hat{\omega}$ represents the maximum angular displacement of latitudinal libration with $0 < \hat{\omega} < 2$. This study is only concerned with some key mathematical properties of finite element method for simulating librationally driven flow in a triaxial ellipsoidal cavity.

In the mantle frame of reference, the dynamics of latitudinally librational driven flow, under the assumptions $Po \ll 1$ and $(Po/\hat{\omega}) \ll 1$, is governed by the dimensional equations:

$$\begin{aligned}\frac{\partial \mathbf{u}}{\partial t} + \mathbf{u}\cdot\nabla\mathbf{u} + 2\Omega_0\left[\hat{\mathbf{z}} + \hat{\mathbf{x}}Po\sin(\Omega_0\hat{\omega}t) - \hat{\mathbf{y}}\,(Po/\hat{\omega})\cos(\Omega_0\hat{\omega}t)\right]\times\mathbf{u} + \frac{1}{\rho}\nabla p \\ = \nu\nabla^2\mathbf{u} + Po\Omega_0^2\left[\hat{\omega}\mathbf{r}\times\hat{\mathbf{x}}\cos(\Omega_0\hat{\omega}t) + \mathbf{r}\times(\hat{\mathbf{z}}\times\hat{\mathbf{x}})\sin(\Omega_0\hat{\omega}t)\right], \qquad (3)\\ \nabla\cdot\mathbf{u} = 0, \qquad (4)\end{aligned}$$

where $\mathbf{r}$ is the position vector, $(\hat{\mathbf{x}}, \hat{\mathbf{y}}, \hat{\mathbf{z}})$ denotes the corresponding unit vectors for the Cartesian coordinates (x, y, z), p is a reduced pressure and $\mathbf{u}$ is the three-dimensional velocity field. The final two terms on the right-hand side of (3) are known as the Poincaré force which results from latitudinal libration and drives fluid motion. Employing the semi axis a as the length scale, Ω_0^{-1} as the unit of time and $\rho a^2\Omega_0^2$ as the unit of pressure, the non-dimensional envelope of a triaxial ellipsoidal cavity is then described by

$$\frac{x^2}{1} + \frac{y^2}{1+\mathcal{E}^2} + \frac{z^2}{1-\mathcal{E}^2} = 1, \tag{5}$$

while the non-dimensional governing equations are

$$\begin{aligned}\frac{\partial \mathbf{u}}{\partial t} + \mathbf{u}\cdot\nabla\mathbf{u} + 2\hat{\mathbf{z}}\times\mathbf{u} + \nabla p \\ = E\nabla^2\mathbf{u} + 2Po\left[(1/\hat{\omega})\,\hat{\mathbf{y}}\times\mathbf{u}\cos(\hat{\omega}t) - \hat{\mathbf{x}}\times\mathbf{u}\sin(\hat{\omega}t)\right] \\ + Po\left[\hat{\omega}\mathbf{r}\times\hat{\mathbf{x}}\cos(\hat{\omega}t) + \mathbf{r}\times(\hat{\mathbf{z}}\times\hat{\mathbf{x}})\sin(\hat{\omega}t)\right], \qquad (6)\\ \nabla\cdot\mathbf{u} = 0. \qquad (7)\end{aligned}$$

Note that the centrifugal force is combined with all other conservative forces to form the reduced pressure p. Librationally driven flow on the bounding

surface, $\mathcal{S}$, of the triaxial ellipsoidal cavity (5) is at rest, requiring that

$$\hat{\mathbf{n}} \cdot \mathbf{u} = 0 \tag{8}$$

and

$$\hat{\mathbf{n}} \times \mathbf{u} = \mathbf{0}, \tag{9}$$

where $\hat{\mathbf{n}}$ denotes the normal to the bounding surface, $\mathcal{S}$, of the ellipsoidal cavity. The problem defined by (6) and (7) subject to the boundary conditions (8) and (9) for triaxial ellipsoidal geometry (5) will be solved subject to the initial condition

$$\mathbf{u}(\mathbf{r}, 0) = \mathbf{u}_0(\mathbf{r})$$

by direct three-dimensional simulation using a finite element method.

3 FINITE ELEMENT METHOD WITH FIRST-ORDER TEMPORAL SCHEME

3.1 Theoretical Preliminaries

For the sake of exposition, we shall rewrite the governing equations in the form

$$\frac{\partial \mathbf{u}}{\partial t} + \mathbf{u} \cdot \nabla \mathbf{u} + \mathbf{Z}(\hat{\omega}, t) \times \mathbf{u} + \nabla p = E \nabla^2 \mathbf{u} + \mathbf{f}(\hat{\omega}, x, y, z, t), \tag{10}$$

$$\nabla \cdot \mathbf{u} = 0, \tag{11}$$

where

$$\mathbf{Z}(\hat{\omega}, t) = 2 \left[\hat{\mathbf{z}} + Po \hat{\mathbf{x}} \sin(\hat{\omega}\, t) - Po \hat{\omega}^{-1} \hat{\mathbf{y}} \cos(\hat{\omega}\, t) \right]$$

and

$$\mathbf{f}(\hat{\omega}, x, y, z, t) = P_0 \Big[\hat{\omega}\, \mathbf{r} \times \hat{\mathbf{x}} \cos(\hat{\omega}\, t) + \mathbf{r} \times (\hat{\mathbf{z}} \times \mathbf{x}) \sin(\hat{\omega}\, t) \Big].$$

We also introduce the following trilinear functional

$$d(\mathbf{w}, \mathbf{u}, \mathbf{v}) = \frac{1}{2} \{ (\mathbf{w} \cdot \nabla \mathbf{u}, \mathbf{v}) - (\mathbf{w} \cdot \nabla \mathbf{v}, \mathbf{u}) \} \quad \forall\, \mathbf{w}, \mathbf{u}, \mathbf{v} \in \mathbf{H}_0^1(\Omega), \tag{12}$$

where (g, h) means the inner product of the two functions g and h. For the coupled system (10) and (11) governing the flow $\mathbf{u}$ and the pressure p in the triaxial ellipsoid Ω, we are interested in its variational formulation: Find $\mathbf{u} \in L^\infty(0, T; L^2(\Omega)^3) \cap L^2(0, T; \mathbf{H}_0^1(\Omega))$ and $p \in L^2(0, T; L_0^2(\Omega))$ such that

$$(\frac{\partial \mathbf{u}}{\partial t}, \mathbf{v}) + E(\nabla \mathbf{u}, \nabla \mathbf{v}) - (p, \nabla \cdot \mathbf{v}) + d(\mathbf{u}, \mathbf{u}, \mathbf{v}) + (\mathbf{Z} \times \mathbf{u}, \mathbf{v})$$
$$= (\mathbf{f}, \mathbf{v}) \quad \forall\, \mathbf{v} \in L^2(0, T; \mathbf{H}_0^1(\Omega)), \tag{13}$$
$$-(\nabla \cdot \mathbf{u}, q) = 0 \quad \forall\, q \in L^2(0, T; L_0^2(\Omega)). \tag{14}$$

We first introduce a few auxiliary inequalities and estimates which will be used in the later analysis. For the trilinear functional $d(\mathbf{w}, \mathbf{u}, \mathbf{v})$, we can easily check that for all $\mathbf{w}, \mathbf{u}, \mathbf{v} \in \mathbf{H}_0^1(\Omega)$,

$$d(\mathbf{w}, \mathbf{u}, \mathbf{v}) = \frac{1}{2}\{(\mathbf{w} \cdot \nabla \mathbf{u}, \mathbf{v}) - (\mathbf{w} \cdot \nabla \mathbf{v}, \mathbf{u})\} = (\mathbf{w} \cdot \nabla \mathbf{u}, \mathbf{v}) + \frac{1}{2}((\nabla \cdot \mathbf{w})\mathbf{u}, \mathbf{v}). \tag{15}$$

Evidently, for any $\mathbf{w}, \mathbf{u} \in \mathbf{H}_0^1(\Omega)$ we have

$$(\mathbf{Z}(t) \times \mathbf{u}, \mathbf{u}) = 0, \quad d(\mathbf{w}, \mathbf{u}, \mathbf{u}) = 0\,,$$

and for all $\mathbf{w}, \mathbf{u}, \mathbf{v} \in \mathbf{H}_0^1(\Omega)$,

$$|d(\mathbf{w}, \mathbf{u}, \mathbf{v})| \le C\, \|\nabla \mathbf{w}\|_0\, \|\nabla \mathbf{u}\|_0\, \|\nabla \mathbf{v}\|_0\,,$$
$$|d(\mathbf{w}, \mathbf{u}, \mathbf{v})| \le C\, \sqrt{\|\mathbf{w}\|_0\, \|\nabla \mathbf{w}\|_0}\, \|\nabla \mathbf{u}\|_0\, \|\nabla \mathbf{v}\|_0\,,$$

where C is constant, while for all $\mathbf{w}, \mathbf{v} \in \mathbf{H}_0^1(\Omega)$ and $\mathbf{u} \in \mathbf{H}^2(\Omega) \cap \mathbf{H}_0^1(\Omega)$ it holds that

$$|d(\mathbf{w}, \mathbf{u}, \mathbf{v})| \le C\, (\|\mathbf{u}\|_{L^\infty} + \|\nabla \mathbf{u}\|_{L^3}) \|\mathbf{w}\|_0\, \|\nabla \mathbf{v}\|_0\,,$$
$$|d(\mathbf{w}, \mathbf{u}, \mathbf{v})| \le C\, \|\nabla \mathbf{w}\|_0 (\|\mathbf{u}\|_{L^\infty} + \|\nabla \mathbf{u}\|_{L^3}) \|\mathbf{v}\|_0\,.$$

We also need the following simple equality:

$$(\mathbf{u} - \mathbf{v}, \mathbf{u}) = \frac{1}{2}\|\mathbf{u}\|_0^2 - \frac{1}{2}\|\mathbf{v}\|_0^2 + \frac{1}{2}\|\mathbf{u} - \mathbf{v}\|_0^2\,,$$

which holds for any vector-valued functions $\mathbf{u}, \mathbf{v} \in \mathbf{R}^n$ and the estimate $|\mathbf{a} \times \mathbf{b}| \le \sqrt{2}|\mathbf{a}|\,|\mathbf{b}|$ which holds for any two vectors $\mathbf{a}, \mathbf{b} \in L^2(\Omega)^3$.

Next we discuss the discretization of the variational system (13) and (14). We start with the partition of the time interval [0, T] and the triangulation of the physical ellipsoidal domain Ω. We divide the time interval [0, T] into M equally spaced subintervals using the following nodal points

$$0 = t_0 < t_1 < t_2 < \ldots < t_M = \mathrm{T},$$

where $t_n = n\,\tau$ for $n = 0, 1, \ldots, M$ and $\tau = T/M$. For any given discrete time sequence $\{\mathbf{u}^n\}_{n=0}^M$ with each $\mathbf{u}^n$ lying in $L^2(\Omega)$ or $L^2(\Omega)^3$, we define the first

order backward finite differences and the averages as follows:

$$\partial_\tau \mathbf{u}^n = \frac{\mathbf{u}^n - \mathbf{u}^{n-1}}{\tau}, \quad \bar{\mathbf{u}}^n = \frac{1}{\tau}\int_{t_{n-1}}^{t_n} \mathbf{u}(\cdot, s)\,\mathrm{d}s.$$

If $\mathbf{u}(\mathbf{r}, t)$ is a function which is continuous with respect to t, we shall often write $\mathbf{u}^n(\cdot) = \mathbf{u}(\cdot, t_n)$ for $n = 0, 1, \ldots, M$.

We now introduce the triangulation of the ellipsoidal domain Ω. For the sake of technical treatments, we shall assume that the boundary of domain Ω is a closed convex polyhedron; the actual curved boundary case can be treated using some well-developed technicalities for the curved boundary (see., e.g., [3,6]) in combination with the finite element error estimates established here. Then we suppose that $\mathcal{T}_h$ is a quasi-uniform triangulation of the polyhedral domain Ω. Let $\mathbf{V}_h \subset \mathbf{H}_0^1(\Omega)$ and $P_h \subset L_0^2(\Omega)$ be the continuous piecewise quadratic and linear finite element spaces associated with $\mathcal{T}_h$.

We shall need the following approximate divergence-free finite element space $\mathbf{V}_{0h}$:

$$\mathbf{V}_{0h} = \{\mathbf{v}_h \in \mathbf{V}_h; \quad (\nabla \cdot \mathbf{v}_h, q_h) = 0 \quad \forall q_h \in P_h\}.$$

We know from [12–14] that the couple $(\mathbf{V}_h, P_h)$ and $\mathbf{V}_{0h}$ satisfy the following approximation properties:

Property (A). For each $\mathbf{v} \in \mathbf{H}^i(\Omega) \cap \mathbf{H}_0^1(\Omega)$ with $\nabla \cdot \mathbf{v} = 0$ and $q \in H^{i-1}(\Omega) \cap L_0^2(\Omega)$ with $i = 1,\ 2,\ 3$, there exist approximations $\pi_h \mathbf{v} \in \mathbf{V}_{0h}$ and $\rho_h q \in P_h$ such that

$$\|\nabla(\mathbf{v} - \pi_h \mathbf{v})\|_0 \le c h^{i-1} \|\mathbf{v}\|_i, \quad \|q - \rho_h q\|_0 \le c h^{i-1} \|q\|_{i-1}.$$

In our subsequent analysis, we shall need the following standard inverse inequality [4]:

$$\|\nabla \mathbf{v}_h\|_0 \le c h^{-1} \|\mathbf{v}_h\|_0, \quad \mathbf{v}_h \in \mathbf{V}_h;$$

and the inf-sup condition [8]: for each $q_h \in P_h$, there exists $\mathbf{v}_h \in \mathbf{V}_h, \mathbf{v}_h \neq 0$ such that

$$d(\mathbf{v}_h, q_h) \ge \beta \|q_h\|_0 \|\nabla \mathbf{v}_h\|_0 .$$

The constants c and β above are positive, depending only on Ω. Also, we shall use a L^2-projection operator from $L^2(\Omega)^3$ to $\mathbf{V}_{0h}$, denoted as I_h. It follows from **Property (A)** that

$$\|\mathbf{v} - I_h \mathbf{v}\|_{0,\Omega} + h\|\nabla(\mathbf{v} - I_h \mathbf{v})\|_{0,\Omega} \le c h^i \|\mathbf{v}\|_{i,\Omega} \quad \forall\, \mathbf{v} \in \mathbf{H}^i(\Omega) \cap \mathbf{V}_0 \qquad (16)$$

for some positive constant c and $i = 1,\ 2,\ 3$, with $\mathbf{V}_0 = \{\mathbf{v} \in \mathbf{H}_0^1(\Omega); \nabla\cdot\mathbf{v} = 0\}$.

Using the first order semi-implicit scheme, we can now formulate the finite element approximation of the system (13) and (14):

Find $\{\mathbf{u}_h^n\} \subset \mathbf{V}_h$ and $\{p_h^n\} \subset P_h$ for $n = 0, 1, \cdots, M$ such that $\mathbf{u}_h^0 = I_h\mathbf{u}_0$ and

$$(\partial_\tau \mathbf{u}_h^n, \mathbf{v}_h) + E(\nabla\mathbf{u}_h^n, \nabla\mathbf{v}_h) - (p_h^n, \nabla\cdot\mathbf{v}_h) + d(\mathbf{u}_h^{n-1}, \mathbf{u}_h^n, \mathbf{v}_h) \tag{17}$$
$$+(\mathbf{Z}^n \times \mathbf{u}_h^n, \mathbf{v}_h) = (\mathbf{f}^n, \mathbf{v}_h) \quad \forall\, \mathbf{v}_h \in \mathbf{V}_h$$
$$-(\nabla\cdot\mathbf{u}_h^n, q_h) = 0 \quad \forall\, q_h \in P_h. \tag{18}$$

We refer to the classic monographs [7,8,22] for basic finite element approximations of the standard Navier-Stokes equations. In the case of the fully discrete finite element approximation of the two-dimensional Navier-Stokes equations, we refer to [10] and [11] for the first order semi-implicit and implicit/explicit temporal schemes and for the stability and convergence under the restrictions $\tau \le C|\ln h|^{-1}$ and $\tau \le C$ with the regularity of $\mathbf{u} \in L^\infty(0,T;\mathbf{H}^2)$ and $p \in L^\infty(0,T;H^1)$. Here we will demonstrate the stability and optimal convergence of the finite element solution $(\mathbf{u}_h^n, p_h^n)$ to the first order semi-implicit scheme (17) and (18) in three dimensions without having any restriction on the time step size τ under the following regularities for the exact solution $(\mathbf{u}, p)$:

(A1) $\mathbf{u} \in L^\infty(0,T;\mathbf{H}^2(\Omega)) \cap L^2(0,T;\mathbf{H}^3(\Omega))$,
$p \in L^2(0,T;H^2(\Omega))$, $\mathbf{u}_t \in L^2(0,T;\mathbf{H}_0^1(\Omega))$.

Remark. If domain Ω is sufficiently smooth, **(A1)** can be derived from the Navier-Stokes equations and the condition $\mathbf{u} \in L^\infty(0,T;\mathbf{H}^2)$ and $p \in L^\infty(0,T;H^1)$.

3.2 Stability and error estimates of finite element solutions

In this section we establish the stability and error estimates of the discrete solution $\{\mathbf{u}_h^n, p_h^n\}$ to the finite element system (17) and (18).

First for the stability, we take $\mathbf{v}_h = \tau\mathbf{u}_h^n$ in (17) to derive

$$\frac{1}{2}\|\mathbf{u}_h^n\|_0^2 - \frac{1}{2}\|\mathbf{u}_h^{n-1}\|_0^2 + \frac{1}{2}\tau^2\|\partial_\tau\mathbf{u}_h^n\|_0^2 + E\,\tau\,\|\nabla\mathbf{u}_h^n\|_0^2 \le \tau\|\mathbf{f}^n\|_0\,\|\mathbf{u}_h^n\|_0\,,$$

then summing over $n = 1, 2, \cdots, k \le M$ and using the Poincaré and Young's inequalities, we obtain the stability estimate:

$$\max_{1\le n\le M}\|\mathbf{u}_h^n\|_0^2+\sum_{n=1}^{M}\left(\tau^2\|\partial_\tau\mathbf{u}_h^n\|_0^2+E\tau\|\nabla\mathbf{u}_h^n\|_0^2\right)\le C(\|\mathbf{u}_h^0\|_0^2+\sum_{n=1}^{M}\tau\|\mathbf{f}^n\|_0^2)\,. \quad (19)$$

Next, we demonstrate that the finite element solution $\{\mathbf{u}_h^n, p_h^n\}$ has the optimal error estimates, as stated in the following theorem.

Theorem 3.1 *Let $(\mathbf{u}, p)$ be the solution to the variational system (13) and (14) with the regularities* **(A1)**, *and $\{(\mathbf{u}_h^n, p_h^n)\}$ be the fully discrete solution to the finite element system (17) and (18). Then we have the following optimal error estimates*

$$\max_{1\le n\le M}\|\mathbf{u}_h^n-\mathbf{u}^n\|_0^2+\tau E\sum_{n=1}^{M}\|\nabla(\mathbf{u}_h^n-\mathbf{u}^n)\|_0^2\le C(\tau^2+h^4)\,. \quad (20)$$

Proof. It suffices to derive the estimate for $\mathbf{u}_h^n-\mathrm{I}_h\mathbf{u}^n$ by using the relation

$$\mathbf{u}_h^n-\mathbf{u}^n=(\mathbf{u}_h^n-\mathrm{I}_h\mathbf{u}^n)+(\mathrm{I}_h\mathbf{u}^n-\mathbf{u}^n) \quad (21)$$

and the triangle inequality and the projection approximation (16). So we will estimate $\mathbf{u}_h^n-\mathrm{I}_h\mathbf{u}^n$ below, and set $\varepsilon_h^n=\mathbf{u}_h^n-\mathrm{I}_h\mathbf{u}^n$.

Integrating both sides of (13) and (14) over the time interval (t_{n-1}, t_n) respectively, we deduce for any $\mathbf{v}\in\mathbf{H}_0^1(\Omega)$ and $q\in L^2(0,T;L_0^2(\Omega))$,

$$(\partial_\tau\mathbf{u}^n,\mathbf{v})+E(\nabla\bar{\mathbf{u}}^n,\nabla\mathbf{v})-(\bar{p}^n,\nabla\cdot\mathbf{v})+(\overline{\mathbf{u}\cdot\nabla\mathbf{u}}^{\,n},\mathbf{v})+(\overline{\mathbf{Z}\times\mathbf{u}}^{\,n},\mathbf{v})=(\bar{\mathbf{f}}^n,\mathbf{v}), \quad (22)$$

and

$$-(\nabla\cdot\bar{\mathbf{u}}^n,q)=0\,. \quad (23)$$

Subtracting (22) from (17), we get the following equation for ε_h^n:

$$\begin{aligned}&(\partial_\tau\varepsilon_h^n,\mathbf{v}_h)+E(\nabla\varepsilon_h^n,\nabla\mathbf{v}_h)-(p_h^n-\bar{p}^n,\nabla\cdot\mathbf{v}_h)\\&=(\mathbf{f}^n-\bar{\mathbf{f}}^n,\mathbf{v}_h)+\left(\overline{\mathbf{u}\cdot\nabla\mathbf{u}}^{\,n}-\mathbf{u}_h^{n-1}\cdot\nabla\mathbf{u}_h^n,\mathbf{v}_h\right)+\left(\overline{\mathbf{Z}\times\mathbf{u}}^{\,n}-\mathbf{Z}^n\times\mathbf{u}_h^n,\mathbf{v}_h\right)\\&+E(\nabla(\bar{\mathbf{u}}^n-\mathrm{I}_h\mathbf{u}^n),\nabla\mathbf{v}_h)\,.\end{aligned}$$

Taking $\mathbf{v}_h^n=\tau\varepsilon_h^n$, we obtain

$$
\begin{aligned}
&\frac{1}{2}\|\varepsilon_h^n\|_0^2-\frac{1}{2}\|\varepsilon_h^{n-1}\|_0^2+\tau E\|\nabla\varepsilon_h^n\|_0^2\equiv\sum_{i=1}^{10}(\mathrm{I})_i\\
&\quad=\int_{t_{n-1}}^{t_n}(t-t_{n-1})(\mathbf{f}_t(t),\varepsilon_h^n)dt-\int_{t_{n-1}}^{t_n}(t-t_{n-1})d_t(\mathbf{u},\mathbf{u},\varepsilon_h^n)dt\\
&\quad+\tau d(\mathbf{u}(t_n)-\mathbf{u}(t_{n-1}),\mathbf{u}(t_n),\varepsilon_h^n)+d(\mathbf{u}(t_{n-1})-I_h\mathbf{u}(t_{n-1})+\varepsilon_h^{n-1},\mathbf{u}(t_n),\varepsilon_h^n)\\
&\quad+\tau d(\mathbf{u}_h^{n-1},\mathbf{u}(t_n)-I_h\mathbf{u}(t_n),\varepsilon_h^n)+\tau(\rho_h\bar{p}^n-\bar{p}^n,\nabla\cdot\varepsilon_h^n)\\
&\quad+\int_{t_{n-1}}^{t_n}(t-t_{n-1})(\mathbf{Z}_t\times\mathbf{u}+\mathbf{Z}\times\mathbf{u}_t,\varepsilon_h^n)dt+(\mathbf{Z}(t_n)\times(\mathbf{u}(t_n)-I_h\mathbf{u}(t_n)),\varepsilon_h^n)\\
&\quad-E\int_{t_{n-1}}^{t_n}(t-t_{n-1})(\nabla\mathbf{u}_t,\nabla\varepsilon_h^n)dt+E\tau(\nabla(\mathbf{u}(t_n)-I_h\mathbf{u}(t_n)),\nabla\varepsilon_h^n),\qquad(24)
\end{aligned}
$$

where, by some standard techniques using the Hölder, Poincaré and Young inequalities, we can derive all estimates from $(\mathrm{I})_1$ to $(\mathrm{I})_{10}$ as follows:

$$
\begin{aligned}
&(\mathrm{I})_1\le C\tau^{\frac{3}{2}}(\int_{t_{n-1}}^{t_n}\|\mathbf{f}_t\|_0^2dt)^{\frac{1}{2}}\|\varepsilon_h^n\|_0\le\frac{E}{16}\|\nabla\varepsilon_h^n\|_0^2\tau+C\tau^2\int_{t_{n-1}}^{t_n}\|\mathbf{f}_t\|_0^2dt,\\
&(\mathrm{I})_2\le C\tau^{\frac{3}{2}}(\int_{t_{n-1}}^{t_n}\|\mathbf{u}_t\|_0^2\|\mathbf{u}\|_2^2dt)^{\frac{1}{2}}\|\nabla\varepsilon_h^n\|_0\le\frac{E}{16}\|\nabla\varepsilon_h^n\|_0^2\tau+C\tau^2\int_{t_{n-1}}^{t_n}\|\mathbf{u}_t\|_0^2\|\mathbf{u}\|_2^2dt,\\
&(\mathrm{I})_3\le C\tau^{\frac{3}{2}}(\int_{t_{n-1}}^{t_n}\|\mathbf{u}_t\|_0^2dt)^{\frac{1}{2}}\|\mathbf{u}(t_n)\|_2\|\nabla\varepsilon_h^n\|_0\le\frac{E}{16}\|\nabla\varepsilon_h^n\|_0^2\tau+C\tau^2\int_{t_{n-1}}^{t_n}\|\mathbf{u}_t\|_0^2\|\mathbf{u}(t_n)\|_2^2dt,\\
&(\mathrm{I})_4\le C\tau\|\varepsilon_h^{n-1}\|_0\|\mathbf{u}(t_n)\|_2\|\nabla\varepsilon_h^n\|_0+C\tau\|\nabla(\mathbf{u}(t_{n-1})-I_h\mathbf{u}(t_{n-1}))\|_0\|\nabla\mathbf{u}(t_n)\|_0\|\nabla\varepsilon_h^n\|_0\\
&\qquad\le\frac{E}{16}\|\nabla\varepsilon_h^n\|_0^2\tau+C\tau\|\nabla(\mathbf{u}(t_{n-1})-I_h\mathbf{u}(t_{n-1}))\|_0^2\|\nabla\mathbf{u}(t_n)\|_0^2+c\tau\|\varepsilon_h^{n-1}\|_0^2\|\mathbf{u}(t_n)\|_2^2,\\
&(\mathrm{I})_5\le Ch^{-1}\tau\|\varepsilon_h^{n-1}\|_0\|\nabla(\mathbf{u}(t_n)-I_h\mathbf{u}_(t_n))\|_0\|\nabla\varepsilon_h^n\|_0\\
&\qquad+C\tau\|\nabla(I_h\mathbf{u}(t_{n-1})\|_0\|\nabla(\mathbf{u}(t_n)-I_h\mathbf{u}(t_n))\|_0\|\nabla\varepsilon_h^n\|_0\\
&\qquad\le\frac{E}{16}\|\nabla\varepsilon_h^n\|_0^2\tau+C\tau\|\nabla\mathbf{u}(t_{n-1})\|_0\|\nabla(\mathbf{u}(t_n)-I_h\mathbf{u}(t_n))\|_0^2+C\tau\|\varepsilon_h^{n-1}\|_0^2\|\mathbf{u}(t_n)\|_2^2,\\
&(\mathrm{I})_6\le C\tau\|\bar{p}^n-\rho_h\bar{p}^n\|_0\|\nabla\varepsilon_h^n\|_0\le\frac{E}{16}\|\nabla\varepsilon_h^n\|_0^2\tau+Ch^4\int_{t_{n-1}}^{t_n}\|p\|_2^2dt,\\
&(\mathrm{I})_7\le C\tau^{\frac{3}{2}}(\int_{t_{n-1}}^{t_n}(|\mathbf{Z}_t|^2\|\mathbf{u}\|_0^2+|\mathbf{Z}|^2\|\mathbf{u}_t\|_0^2)dt)^{\frac{1}{2}}\|\nabla\varepsilon_h^n\|_0\\
&\qquad\le\frac{E}{16}\|\nabla\varepsilon_h^n\|_0^2\tau+C\tau^2\int_{t_{n-1}}^{t_n}(|\mathbf{Z}_t|^2\|\mathbf{u}\|_0^2+|\mathbf{Z}|^2\|\mathbf{u}_t\|_0^2)dt,\\
&(\mathrm{I})_8\le C\tau|\mathbf{Z}(t_n)|\|\mathbf{u}(t_n)-I_h\mathbf{u}(t_n)\|_0\|\varepsilon_h^n\|_0\\
&\qquad\le\frac{E}{16}\|\nabla\varepsilon_h^n\|_0^2\tau+C\tau|\mathbf{Z}(t_n)|^2\|\nabla(\mathbf{u}(t_n)-I_h\mathbf{u}(t_n))\|_0^2,\\
&(\mathrm{I})_9\le C\tau^{\frac{3}{2}}(\int_{t_{n-1}}^{t_n}\|\nabla\mathbf{u}_t\|_0^2dt)^{\frac{1}{2}}\|\nabla\varepsilon_h^n\|_0\le\frac{E}{16}\|\nabla\varepsilon_h^n\|_0^2\tau+C\tau^2\int_{t_{n-1}}^{t_n}\|\nabla\mathbf{u}_t\|_0^2dt,\\
&(\mathrm{I})_{10}\le C\tau\|\nabla(\mathbf{u}(t_n)-I_h\mathbf{u}(t_n))\|_0\|\nabla\varepsilon_h^n\|_0\le\frac{E}{16}\|\nabla\varepsilon_h^n\|_0^2\tau+C\tau\|\nabla(\mathbf{u}(t_n)-\mathbf{u}(t_n))\|_0^2.
\end{aligned}
$$

Summing (24) from $n=1$ to $n=m$ and using the above estimates and the regularities **(A1)**, we obtain

$$\|\varepsilon_h^m\|_0^2 + E\tau \sum_{n=1}^{m} \|\nabla \varepsilon_h^n\|_0^2 \le C(\tau^2 + h^4) \int_0^T \Big(\|\mathbf{f}_t\|_0^2 + \|\mathbf{u}\|_0^2 + \|\mathbf{u}_t\|_1^2 + \|p\|_2^2 \Big) dt$$
$$+ C\tau \sum_{n=1}^{M} \|\nabla(\mathbf{u}(t_n) - I_h\mathbf{u}(t_n))\|_0^2 + C\tau \sum_{n=1}^{m-1} \|\mathbf{u}(t_{n+1})\|_2^2 \|\varepsilon_h^n\|_0^2. \tag{25}$$

Applying the Gronwall lemma to (25) and using **(A1)**, we further deduce

$$\begin{aligned}
&\|\varepsilon_h^m\|_0^2 + E\tau \sum_{n=1}^{m} \|\nabla \varepsilon_h^n\|_0^2 \\
&\qquad \le \exp\{C\tau \sum_{n=1}^{m-1} \|\mathbf{u}(t_{n+1})\|_2^2\} \{C(\tau^2 + h^4) \int_0^T [\|\mathbf{f}_t\|_0^2 + \|\mathbf{u}\|_0^2 + \|\mathbf{u}_t\|_1^2 + \|p\|_2^2] dt \\
&\qquad + \exp\{C\tau \sum_{n=1}^{m-1} \|\mathbf{u}(t_{n+1})\|_2^2\} C\tau \sum_{n=1}^{M} \|\nabla(\mathbf{u}(t_n) - I_h\mathbf{u}(t_n))\|_0^2.
\end{aligned} \tag{26}$$

Noting

$$\begin{aligned}
&\tau \|\nabla(\mathbf{u}(t_n) - I_h\mathbf{u}(t_n))\|_0^2 \\
&\quad \le 3\tau \|\nabla(\mathbf{u}(t_n) - \bar{\mathbf{u}}^n)\|_0^2 + 3\tau \|\nabla(\bar{\mathbf{u}}^n - I_h\bar{\mathbf{u}}^n)\|_0^2 + 3\tau \|\nabla(I_h\bar{\mathbf{u}}^n - I_h\mathbf{u}(t_n))\|_0^2 \\
&\quad \le C\tau \|\nabla(\mathbf{u}(t_n) - \bar{\mathbf{u}}^n)\|_0^2 + C\tau \|\nabla(\bar{\mathbf{u}}^n - I_h\bar{\mathbf{u}}^n)\|_0^2 \\
&\quad \le C\tau^2 \int_{t_{n-1}}^{t_n} \|\nabla \mathbf{u}_t\|_0^2 dt + Ch^4\tau \|\bar{u}^n\|_3^2 \\
&\quad \le C(\tau^2 + h^4) \int_{t_{n-1}}^{t_n} [\|\nabla \mathbf{u}_t\|_0^2 + \|\mathbf{u}\|_3^2] dt \,,
\end{aligned} \tag{27}$$

the desired estimate (20) follows from (21) by the triangle inequality, (26) and (27), and the projection approximation (16). ♯

4 A FINITE ELEMENT METHOD WITH SECOND-ORDER TEMPORAL SCHEME

In the previous section we have discussed a fully discrete finite element method with first order time scheme. But for our highly nonlinear libration system, it seems the first order time scheme is not always sufficient to capture the accuracy of the flow in an effective and stable manner. In this section we shall present a more accurate time discretization, the second order Crank-Nicolson scheme. The subsequent notations for the time and space discretizations as well as the finite element spaces are all carried over from the previous section.

Now we are going to use the implicit second order Crank-Nicolson scheme for time derivative and the explicit second order extrapolation to deal with the

nonlinear term, namely the following approximations:

$$\mathbf{u}^{n+1/2} = \left(\frac{3}{2}\mathbf{u}^n - \frac{1}{2}\mathbf{u}^{n-1}\right) + \frac{3}{8}\tau^2\mathbf{u}_{ttt}^{n+1/2} + O(\tau^3)\,,$$
$$\mathbf{u}_t^{n+1/2} = \frac{\mathbf{u}^{n+1} - \mathbf{u}^n}{\tau} - \frac{1}{24}\tau^2\mathbf{u}_{ttt}^{n+1/2} + O(\tau^3)\,.$$

For convenience, we shall also write

$$\bar{\mathbf{u}}^{n+1/2} = \frac{1}{\tau}\int_{t_n}^{t_{n+1}} \mathbf{u}(s)\,\mathrm{d}s\,, \quad \mathbf{u}^{n+1/2} = \frac{\mathbf{u}^{n+1} + \mathbf{u}^n}{2}\,, \quad \mathbf{u}_h^{n+1/2} = \frac{\mathbf{u}_h^{n+1} + \mathbf{u}_h^n}{2}$$

and

$$T_n(\mathbf{u}) = \frac{3}{2}\mathbf{u}^n - \frac{1}{2}\mathbf{u}^{n-1} \quad \text{or} \quad T_n(\mathbf{u}_h) = \frac{3}{2}\mathbf{u}_h^n - \frac{1}{2}\mathbf{u}_h^{n-1}\,.$$

Using these approximations in time along with the same finite element approximations as used in the previous section in space, we propose the following fully discrete finite element scheme for the system (13) and (14):

Find $\{\mathbf{u}_h^n\} \subset \mathbf{V}_h$ and $\{p_h^n\} \subset P_h$ for $n = 0, 1, \cdots, M$ such that $\mathbf{u}_h^0 = \mathrm{I}_h\mathbf{u}_0$ and

$$\Big(\partial_\tau \mathbf{u}_h^{n+1}, \mathbf{v}_h\Big) + E(\nabla\mathbf{u}_h^{n+1/2}, \nabla\mathbf{v}_h) - (p_h^{n+1/2}, \nabla\cdot\mathbf{v}_h) \tag{28}$$
$$+d\Big(T_n(\mathbf{u}_h), \mathbf{u}_h^{n+1/2}, \mathbf{v}_h\Big) + \Big(\mathbf{Z}^{n+1/2}\times\mathbf{u}_h^{n+1/2}, \mathbf{v}_h\Big) = (\mathbf{f}^{n+1/2}, \mathbf{v}_h) \forall \mathbf{v}_h \in \mathbf{V}_h,$$
$$-(\nabla\cdot\mathbf{u}_h^{n+1/2}, q_h) = 0 \quad \forall\, q_h \in P_h. \tag{29}$$

Here we shall establish for the first time the stability and optimal convergence of the discrete solution $(\mathbf{u}_h^n, p_h^n)$ to the finite element system (28) and (29) in three dimensions without imposing any restriction on the time step size τ under the following regularities on the exact solution $(\mathbf{u}, p)$:

$$(\mathbf{A2}) \quad \begin{cases} \mathbf{u} \in L^\infty(0,T;\mathbf{H}^2(\Omega)) \cap L^2(0,T;\mathbf{H}^3(\Omega)), \quad p \in L^2(0,T;H^2(\Omega)), \\ \mathbf{u}_t \in L^\infty(0,T;\mathbf{H}^1(\Omega)) \cap L^2(0,T;\mathbf{H}^2(\Omega)),\ \mathbf{u}_{tt} \in L^2(0,T;\mathbf{H}^1(\Omega)). \end{cases}$$

4.1 Stability and error estimates of finite element solutions

In this section we establish the stability and error estimate of the discrete solutions $\{\mathbf{u}_h^n, p_h^n\}$ to the finite element system (28) and (29).

First for the stability, we choose $\mathbf{v}_h = \tau\mathbf{u}_h^{n+1/2}$ in (28) to obtain

$$\frac{1}{2}\|\mathbf{u}_h^{n+1}\|_0^2 - \frac{1}{2}\|\mathbf{u}_h^n\|_0^2 + E\,\tau\,\|\nabla\mathbf{u}_h^{n+1/2}\|_0^2 \le \frac{E}{2}\|\nabla\mathbf{u}_h^n\|_0^2 + C\tau\|\mathbf{f}^{n+1/2}\|_0^2\,,$$

then summing over $n = 1, 2, \cdots, k \le M$, we derive the stability estimate:

$$\max_{1\le n\le M} \|\mathbf{u}_h^n\|_0^2 + E\sum_{n=1}^{M} \tau \|\nabla \mathbf{u}_h^{n+1/2}\|_0^2 \le C(\|\mathbf{u}_h^0\|_0^2 + \sum_{n=1}^{M} \tau \|\mathbf{f}^n\|_0^2)\,. \tag{30}$$

In the remainder of this section we will demonstrate the optimal error estimate of the finite element solutions $\{\mathbf{u}_h^n, p_h^n\}$ to the system (28) and (29), as stated in the following theorem.

Theorem 4.1 *Let $(\mathbf{u}, p)$ be the solution to the variational system (13) and (14) with the regularities* **(A2)**, *and $\{(\mathbf{u}_h^n, p_h^n)\}$ be the fully approximate solution to the finite element system (28) and (29). Then we have the following optimal error estimates*

$$\max_{1\le n\le M} \|\mathbf{u}_h^n - \mathbf{u}^n\|_0^2 + \tau E\sum_{n=1}^{M} \|\nabla(\mathbf{u}_h^n - \mathbf{u}^n)\|_0^2 \le C(\tau^4 + h^4)\,. \tag{31}$$

Proof. Similarly as we argued in the proof of Theorem 3.1, it suffices to estimate the error $\varepsilon_h^n = \mathbf{u}_h^n - \mathrm{I}_h\mathbf{u}^n$. To derive the equation satisfied by ε_h^n, we integrate both sides of (13) and (14) over the time interval (t_n, t_{n+1}) respectively to deduce for any $\mathbf{v} \in \mathbf{H}_0^1(\Omega)$ and $q \in L_0^2(\Omega)$,

$$\begin{aligned}
&(\partial_\tau \mathbf{u}^{n+1}, \mathbf{v}) + E(\nabla \bar{\mathbf{u}}^{n+1/2}, \nabla \mathbf{v}) - (\bar{p}^{n+1/2}, \nabla\cdot\mathbf{v}) + (\overline{\mathbf{u}\cdot\nabla\mathbf{u}}^{\,n+1/2}, \mathbf{v})\\
&\quad + (\overline{\mathbf{Z}\times\mathbf{u}}^{\,n+1/2}, \mathbf{v}) = (\bar{\mathbf{f}}^{n+1/2}, \mathbf{v})\,, &(32)\\
&\quad -(\nabla\cdot\bar{\mathbf{u}}^{n+1/2}, q) = 0. &(33)
\end{aligned}$$

Subtracting (32) from (28) we obtain the following equation for the error function ε_h^n:

$$\begin{aligned}
&(\partial_\tau \varepsilon_h^{n+1}, \mathbf{v}_h) + E(\nabla \varepsilon_h^{n+1/2}, \nabla \mathbf{v}_h) - (p_h^{n+1/2} - \bar{p}^{n+1/2}, \nabla\cdot\mathbf{v}_h)\\
&= (\mathbf{f}^{n+1/2} - \bar{\mathbf{f}}^{n+1/2}, \mathbf{v}_h) + \left(\overline{\mathbf{u}\cdot\nabla\mathbf{u}}^{\,n+1/2} - T_n(\mathbf{u}_h)\cdot\nabla\mathbf{u}_h^{n+1/2}, \mathbf{v}_h\right)\\
&\quad + \left(\overline{\mathbf{Z}\times\mathbf{u}}^{\,n+1/2} - \mathbf{Z}^{n+1/2}\times\mathbf{u}_h^{n+1/2}, \mathbf{v}_h\right) + (\partial_\tau(\mathbf{u}^{n+1} - \mathrm{I}_h\mathbf{u}^{n+1}), \mathbf{v}_h)\\
&\quad + E(\nabla(\bar{\mathbf{u}}^{n+1/2} - \mathrm{I}_h\mathbf{u}^{n+1/2}), \nabla\mathbf{v}_h)\,.
\end{aligned}$$

Taking $\mathbf{v}_h^n = \tau\varepsilon_h^{n+1/2}$ in the above equation and using the approximation property (16) of projection I_h, we can write

$$
\begin{aligned}
&\frac{1}{2}\|\varepsilon_h^{n+1}\|_0^2-\frac{1}{2}\|\varepsilon_h^{n}\|_0^2+\tau E\|\nabla\varepsilon_h^{n+1/2}\|_0^2\equiv\sum_{i=1}^{12}(\mathrm{I})_i\\
&\quad=\frac{1}{2}\int_{t_n}^{t_{n+1}}(t-t_n)(t_{n+1}-t)(\mathbf{f}_{tt},\varepsilon_h^{n+1/2})dt\\
&\quad-\frac{1}{2}\int_{t_n}^{t_{n+1}}(t-t_n)(t_{n+1}-t)(\mathbf{Z}_{tt}\times\mathbf{u}+2\mathbf{Z}_t\times\mathbf{u}_t+\mathbf{Z}\times\mathbf{u}_{tt},\varepsilon_h^{n+\frac{1}{2}})\\
&\quad+\frac{\tau}{4}((\mathbf{Z}(t_{n+1})-\mathbf{Z}(t_n))\times(\mathbf{u}(t_{n+1})-\mathbf{u}(t_n)),\varepsilon_h^{n+\frac{1}{2}})\\
&\quad+\tau(\mathbf{Z}^{n+\frac{1}{2}}\times(\mathbf{u}^{n+\frac{1}{2}}-I_h\mathbf{u}^{n+\frac{1}{2}}),\varepsilon_h^{n+\frac{1}{2}})\\
&\quad-\frac{E}{2}\int_{t_n}^{t_{n+1}}(t-t_n)(t_{n+1}-t)(\nabla\mathbf{u}_{tt},\nabla\varepsilon_h^{n+\frac{1}{2}})dt+E\tau(\nabla(\mathbf{u}^{n+\frac{1}{2}}-I_h\mathbf{u}^{n+\frac{1}{2}}),\nabla\varepsilon_h^{n})\\
&\quad+\tau(\rho_h\bar{p}^{n+\frac{1}{2}}-\bar{p}^{n+\frac{1}{2}},\nabla\cdot\varepsilon_h^{n+\frac{1}{2}})-\frac{1}{2}\int_{t_n}^{t_{n+1}}(t-t_n)(t_{n+1}-t)d_{tt}(\mathbf{u},\mathbf{u},\varepsilon_h^{n+\frac{1}{2}})dt\\
&\quad+\frac{\tau}{4}d(\mathbf{u}(t_{n+1})-\mathbf{u}(t_n),\mathbf{u}(t_{n+1})-\mathbf{u}(t_n),\varepsilon_h^{n})\\
&\quad+\frac{\tau}{2}d(\mathbf{u}(t_{n+1}-2\mathbf{u}(t_n)+\mathbf{u}(t_{n-1}),\mathbf{u}^{n+\frac{1}{2}},\varepsilon_h^{n+\frac{1}{2}})\\
&+\tau d(T_n(\mathbf{u})-I_hT_n(\mathbf{u})+T_n(\varepsilon_h),\mathbf{u}^{n+\frac{1}{2}},\varepsilon_h^{n+\frac{1}{2}})+\tau d(T_n(\mathbf{u}_h),\mathbf{u}^{n+\frac{1}{2}}-I_h\mathbf{u}^{n+\frac{1}{2}},\varepsilon_h^{n+\frac{1}{2}}),\quad(34)
\end{aligned}
$$

where, by the standard techniques, we can estimate $(\mathrm{I})_1$ to $(\mathrm{I})_7$ as

$$
\begin{aligned}
(\mathrm{I})_1&\le C\tau^{\frac{5}{2}}(\int_{t_n}^{t_{n+1}}\|\|\mathbf{f}_{tt}\|_0^2dt)^{\frac{1}{2}}\|\varepsilon_h^{n+\frac{1}{2}}\|_0\le\frac{E}{16}\|\nabla\varepsilon_h^{n+\frac{1}{2}}\|_0^2\tau+C\tau^4\int_{t_n}^{t_{n+1}}\|\mathbf{f}_{tt}\|_0^2dt,\\
(\mathrm{I})_2&\le C\tau^{\frac{5}{2}}(\int_{t_n}^{t_{n+1}}[|\mathbf{Z}_{tt}|^2\|\mathbf{u}\|_0^2+|\mathbf{Z}_t|^2\|\mathbf{u}_t\|_0^2+|\mathbf{Z}|^2\|\mathbf{u}_{tt}\|_0^2]dt)^{\frac{1}{2}}\|\varepsilon_h^{n+\frac{1}{2}}\|_0\\
&\le\frac{E}{16}\|\nabla\varepsilon_h^{n+\frac{1}{2}}\|_0^2\tau+C\tau^4\int_{t_{n-1}}^{t_n}[\|\mathbf{u}\|_0^2+\|\mathbf{u}_t\|_0^2+\|\mathbf{u}_{tt}\|_0^2]dt,\\
(\mathrm{I})_3&\le C\tau\int_{t_n}^{t_{n+1}}|\mathbf{Z}_t|dt\int_{t_n}^{t_{n+1}}\|\mathbf{u}_t\|_0dt\|\varepsilon_h^{n+\frac{1}{2}}\|_0\\
&\le\frac{E}{16}\|\nabla\varepsilon_h^{n+\frac{1}{2}}\|_0^2\tau+C\tau^4\int_{t_n}^{t_{n+1}}\|\mathbf{u}_t\|_0^2dt,\\
(\mathrm{I})_4&\le C\tau|\mathbf{Z}^{n+\frac{1}{2}}|\|\mathbf{u}^{n+\frac{1}{2}}-I_h\mathbf{u}^{n+\frac{1}{2}}\|_0\|\varepsilon_h^{n+\frac{1}{2}}\|_0\\
&\le\frac{E}{16}\|\nabla\varepsilon_h^{n+\frac{1}{2}}\|_0^2\tau+C\tau\|\nabla(\mathbf{u}^{n+\frac{1}{2}}-I_h\mathbf{u}^{n+\frac{1}{2}})\|_0^2,\\
(\mathrm{I})_5&\le E\tau^{\frac{5}{2}}(\int_{t_n}^{t_{n+1}}\|\nabla\mathbf{u}_{tt}\|_0^2dt)^{\frac{1}{2}}\|\nabla\varepsilon_h^{n+\frac{1}{2}}\|_0\le\frac{E}{16}\|\nabla\varepsilon_h^{n+\frac{1}{2}}\|_0^2\tau+C\tau^4\int_{t_n}^{t_{n+1}}\|\nabla\mathbf{u}_{tt}\|_0^2dt,\\
(\mathrm{I})_6&\le C\tau\|\nabla(\mathbf{u}^{n+\frac{1}{2}}-I_h\mathbf{u}^{n+\frac{1}{2}})\|_0\|\nabla\varepsilon_h^{n+\frac{1}{2}}\|_0\\
&\le\frac{E}{16}\|\nabla\varepsilon_h^{n+\frac{1}{2}}\|_0^2\tau+C\tau\|\nabla(\mathbf{u}^{n+\frac{1}{2}}-I_h\mathbf{u}^{n+\frac{1}{2}})\|_0^2,\\
(\mathrm{I})_7&\le C\tau h^2\|\nabla\varepsilon_h^{n+\frac{1}{2}}\|_0\|\bar{p}^{n+\frac{1}{2}}\|_2\le\frac{E}{16}\|\nabla\varepsilon_h^{n+\frac{1}{2}}\|_0^2\tau+Ch^4\int_{t_n}^{t_{n+1}}\|p\|_2^2dt,
\end{aligned}
$$

while $(\mathrm{I})_8$ to $(\mathrm{I})_{12}$ are in the form

$$
\begin{aligned}
(\mathrm{I})_8 \leq & C\tau^{\frac{5}{2}}\Big(\int_{t_n}^{t_{n+1}}[\|\mathbf{u}_{tt}\|_0^2\|\mathbf{u}\|_2^2+\|\mathbf{u}_t\|_2^2\|\mathbf{u}_t\|_0^2]dt\Big)^{\frac{1}{2}}\|\nabla\varepsilon_h^n\|_0\\
\leq & \frac{E}{16}\|\nabla\varepsilon_h^{n+\frac{1}{2}}\|_0^2\tau+C\tau^4\int_{t_{n-1}}^{t_n}[\|\mathbf{u}_{tt}\|_0^2\|\mathbf{u}\|_2^2+\|\mathbf{u}_t\|_2^2\|\mathbf{u}_t\|_0^2]dt,\\
(\mathrm{I})_9 \leq & C\tau\|\nabla\varepsilon_h^{n+\frac{1}{2}}\|_0\Big(\int_{t_n}^{t_{n+1}}\|\nabla\mathbf{u}_t\|_0dt\Big)^2\\
\leq & \frac{E}{16}\|\nabla\varepsilon_h^{n+\frac{1}{2}}\|_0^2\tau+C\tau^4\sup_{0\leq t\leq T}\|\nabla\mathbf{u}_t(t)\|_0^2\int_{t_n}^{t_{n+1}}\|\nabla\mathbf{u}_t\|_0^2dt,\\
(\mathrm{I})_{10} \leq & C\tau^{\frac{5}{2}}\|\nabla\varepsilon_h^{n+\frac{1}{2}}\|_0\|\mathbf{u}^{n+\frac{1}{2}}\|_2\Big(\int_{t_{n-1}}^{t_{n+1}}\|\mathbf{u}_{tt}\|_0^2dt\Big)^{\frac{1}{2}}\\
\leq & \frac{E}{16}\|\nabla\varepsilon_h^{n+\frac{1}{2}}\|_0^2\tau+C\tau^4\sup_{0\leq t\leq T}\|\mathbf{u}(t)\|_2^2\int_{t_n}^{t_{n+1}}\|\mathbf{u}_{tt}\|_0^2dt,\\
(\mathrm{I})_{11} \leq & C\tau\|\nabla\varepsilon_h^{n+\frac{1}{2}}\|_0(\|\nabla(T_n(\mathbf{u})-I_hT_n(\mathbf{u}))\|_0\|\nabla\mathbf{u}^{n+\frac{1}{2}}\|_0+\|T_n(\varepsilon_h)\|_0\|\mathbf{u}^{n+\frac{1}{2}}\|_2)\\
\leq & \frac{E}{16}\|\nabla\varepsilon_h^{n+\frac{1}{2}}\|_0^2\tau+C\tau\|\nabla(T_n(\mathbf{u})-I_hT_n(\mathbf{u}))\|_0^2\|\nabla\mathbf{u}^{n+\frac{1}{2}}\|_0^2\\
& +C\tau\|T_n(\varepsilon_h)\|_0^2\|\mathbf{u}^{n+\frac{1}{2}}\|_2^2,\\
(\mathrm{I})_{12} \leq & C\tau(h^{-1}\|T_n(\varepsilon_h)\|_0+\|\nabla T_n(I_h\mathbf{u})\|_0)\|\nabla(\mathbf{u}^{n+\frac{1}{2}}-I_h\mathbf{u}^{n+\frac{1}{2}})\|_0\|\nabla\varepsilon_h^{n+\frac{1}{2}}\|_0\\
\leq & \frac{E}{16}\|\nabla\varepsilon_h^{n+\frac{1}{2}}\|_0^2\tau+C\tau\|T_n(\varepsilon_h)\|_0^2\|\mathbf{u}^{n+\frac{1}{2}}\|_2^2\\
& +C\tau\|\nabla T_n(\mathbf{u})\|_0^2\|\nabla(\mathbf{u}^{n+\frac{1}{2}}-I_h\mathbf{u}^{n+\frac{1}{2}})\|_0^2.
\end{aligned}
$$

Summing (34) from $n=1$ to $n=m-1$ and using the above inequalities and the regularities **(A2)** lead to

$$
\begin{aligned}
&\|\varepsilon_h^m\|_0^2+E\tau\sum_{n=1}^{m}\|\nabla\varepsilon_h^n\|_0^2\\
&\quad\leq C(\tau^4+h^4)\int_0^T[\|\mathbf{f}_{tt}\|_0^2+\|\mathbf{u}\|_0^2+\|p\|_2^2+\|\mathbf{u}_t\|_2^2+\|\nabla\mathbf{u}_{tt}\|_0^2]dt\\
&\quad+C\tau\sum_{n=1}^{M-1}[\|\nabla(T_n(\mathbf{u})-I_hT_n(\mathbf{u}))\|_0^2+\|\nabla(\mathbf{u}^{n+\frac{1}{2}}-I_h\mathbf{u}^{n+\frac{1}{2}})\|_0^2]\\
&\quad+\tau\sum_{n=1}^{m-1}d_n\|\varepsilon_h^n\|_0^2,
\end{aligned}
\tag{35}
$$

where we write $d_{M-1}=C(\|\mathbf{u}(t_M)\|_2^2+\|\mathbf{u}(t_{M-1})\|_2^2)$, and

$$
d_n=C(\|\mathbf{u}(t_{n+2})\|_2^2+\|\mathbf{u}(t_{n+1})\|_2^2+\|\mathbf{u}(t_n)\|_2^2)
$$

for $n=1,\cdots,M-2$. On applying the Gronwall lemma to (35) and using the regularities **(A2)**, we deduce

$$
\begin{aligned}
&\|\varepsilon_h^m\|_0^2 + E\tau\sum_{n=1}^{m}\|\nabla\varepsilon_h^n\|_0^2\\
&\quad\le \exp\{\tau\sum_{n=1}^{m-1} d_n\}\Big\{C(\tau^4+h^4)\\
&\quad\times\int_0^T[\|\mathbf{f}_{tt}\|_0^2+\|\mathbf{u}\|_0^2+\|p\|_2^2+\|\mathbf{u}_t\|_2^2+\|\nabla\mathbf{u}_{tt}\|_0^2]dt\\
&\quad+C\tau\sum_{n=1}^{M}[\|\nabla(T_n(\mathbf{u})-I_hT_n(\mathbf{u}))\|_0^2+\|\nabla(\mathbf{u}^{n+\frac12}-I_h\mathbf{u}^{n+\frac12})\|_0^2]\Big\}\\
&\quad\le C(\tau^4+h^4)\int_0^T[\|\mathbf{f}_{tt}\|_0^2+\|\mathbf{u}\|_0^2+\|p\|_2^2+\|\mathbf{u}_t\|_2^2+\|\nabla\mathbf{u}_{tt}\|_0^2]dt\\
&\quad+C\tau\sum_{n=1}^{M}[\|\nabla(T_n(\mathbf{u})-I_hT_n(\mathbf{u}))\|_0^2+\|\nabla(\mathbf{u}^{n+\frac12}-I_h\mathbf{u}^{n+\frac12})\|_0^2]. \qquad (36)
\end{aligned}
$$

But the last two terms in (36) can be estimated as follows:

$$
\begin{aligned}
&\tau\|\nabla(\mathbf{u}^{n+\frac12}-I_h\mathbf{u}^{n+\frac12})\|_0^2\\
&\quad\le 3\tau\|\nabla(\mathbf{u}^{n+\frac12}-\bar{\mathbf{u}}^{n+\frac12})\|_0^2+3\tau\|\nabla(\bar{\mathbf{u}}^{n+\frac12}-I_h\bar{\mathbf{u}}^{n+\frac12})\|_0^2+3\tau\|\nabla(I_h\bar{\mathbf{u}}^{n+\frac12}-I_h\mathbf{u}^{n+\frac12})\|_0^2\\
&\quad\le C\tau\|\nabla(\mathbf{u}^{n+\frac12}-\bar{\mathbf{u}}^{n+\frac12})\|_0^2+C\tau\|\nabla(\bar{\mathbf{u}}^{n+\frac12}-I_h\bar{\mathbf{u}}^{n+\frac12})\|_0^2\\
&\quad\le C\tau^4\int_{t_n}^{t_{n+1}}\|\nabla\mathbf{u}_{tt}\|_0^2dt+Ch^4\tau\|\bar{u}^{n+\frac12}\|_3^2\le C(\tau^4+h^4)\int_{t_n}^{t_{n+1}}[\|\nabla\mathbf{u}_{tt}\|_0^2+\|\mathbf{u}\|_3^2]dt, \quad (37)
\end{aligned}
$$

and

$$
\begin{aligned}
&\tau\|\nabla(T_n(\mathbf{u})-I_hT_n(\mathbf{u}))\|_0^2\\
&\quad=\tau\|\nabla[(\mathbf{u}^{n+\frac12}-\mathbf{u}^{n+\frac12}-T_n(\mathbf{u}))-I_h(\mathbf{u}^{n+\frac12}-\mathbf{u}^{n+\frac12}-T_n(\mathbf{u}))]\|_0^2\\
&\quad\le 3\tau\|\nabla\mathbf{u}^{n+\frac12}-I_h\mathbf{u}^{n+\frac12})\|_0^2+3\tau\|\nabla\int_{t_n}^{t_{n+1}}(\mathbf{u}_t-I_h\mathbf{u}_t)dt\|_0^2\\
&\quad+3\tau\|\nabla\int_{t_{n-1}}^{t_n}(\mathbf{u}_t-I_h\mathbf{u}_t)dt\|_0^2\\
&\quad\le 3\tau\|\nabla(\mathbf{u}^{n+\frac12}-\bar{\mathbf{u}}^{n+\frac12})\|_0^2+C\tau^2h^2\int_{t_n}^{t_{n+1}}\|\mathbf{u}_t\|_2^2dt\\
&\quad\le C(\tau^4+h^4)\int_{t_n}^{t_{n+1}}[\|\nabla\mathbf{u}_{tt}\|_0^2+\|\mathbf{u}_t\|_2^2+\|\mathbf{u}\|_3^2]dt. \qquad (38)
\end{aligned}
$$

Now the desired estimate (31) follows from (21) by the triangle inequality and (36)–(38) and the projection approximation (16). ♯

5 NUMERICAL IMPLEMENTATION AND APPLICATION

5.1 Triaxial ellipsoidal tetrahedral mesh

The essential strategy for generating a tetrahedral mesh suitable for a triaxial ellipsoidal cavity is first to construct a spherical tetrahedral mesh [5] which is then deformed into a triaxial ellipsoidal geometry by introducing the eccentricity $\mathcal{E}$ as a geometric parameter of the triaxial ellipsoidal mesh. More precisely, all nodes (x_i, y_i, z_i) in a spherical tetrahedral mesh within the unit sphere satisfying

$$x_i^2 + y_i^2 + z_i^2 = r_i^2, \qquad 0 < r_i \leq 1,$$

can be transformed by

$$x_i^{\mathcal{E}} = x_i, \quad y_i^{\mathcal{E}} = y_i\sqrt{1+\mathcal{E}^2}, \quad z_i^{\mathcal{E}} = z_i\sqrt{1-\mathcal{E}^2}$$

such that the deformed nodes $(x_i^{\mathcal{E}}, y_i^{\mathcal{E}}, z_i^{\mathcal{E}})$ satisfy

$$(x_i^{\mathcal{E}})^2 + \frac{(y_i^{\mathcal{E}})^2}{1+\mathcal{E}^2} + \frac{(z_i^{\mathcal{E}})^2}{1-\mathcal{E}^2} = r_i^2, \qquad 0 < r_i \leq 1.$$

For the purpose of resolving the thin viscous boundary layer, we can construct more nodes in the vicinity of the bounding surface of the triaxial ellipsoidal cavity by stretching the spherical mesh points (x_i, y_i, z_i) radially before the deformation, for example,

$$\begin{bmatrix} x_i \\ y_i \\ z_i \end{bmatrix} = \frac{1}{r_i}\sin\left(\frac{\pi}{2}r_i\right)^{2/3} \begin{bmatrix} x_i \\ y_i \\ z_i \end{bmatrix}.$$

The spherical mesh itself begins with approximating the sphere by an icosahedron which is then further divided into 20 identical tetrahedra based on its 20 triangular facets and the center of the sphere. This initial tetrahedral mesh is then refined recursively by subdividing each of the tetrahedra into eight subtetrahedra. The three-dimensional tetrahedralization of the triaxial ellipsoid produces a finite element mesh that does not have pole or central numerical singularities. When $\mathcal{E}$ is very close to 1, representing a highly flatted triaxial ellipsoidal disk, an alternative meshing algorithm should be used. This is because a regular shaped tetrahedron after transformation may become too stretched and, consequently, lead to a poor finite element approximation. In this case, a general mesh generation algorithm based on the Delaunay triangulation can be employed instead.

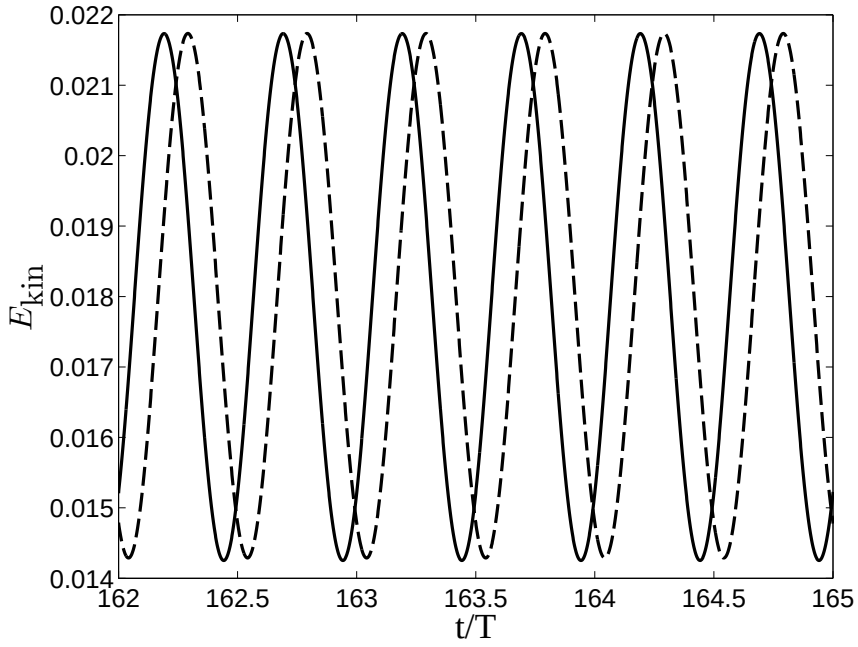

Fig. 1. Kinetic energies, $E_{\rm kin}(t)$, obtained with two different numerical schemes are shown as a function of the scaled time ($T = 2\pi/\hat{\omega}$) at a fixed $\mathcal{E} = 0.5$ for $E = 10^{-4}, \hat{\omega} = 1.2$ and $Po = 0.3$. The solid line is obtained using the implicit scheme while the dashed line from the explicit scheme.

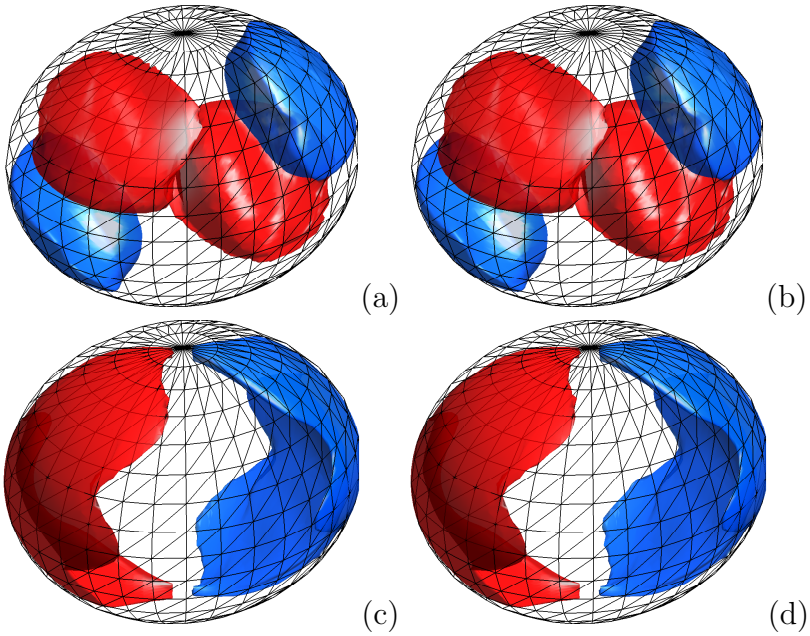

Fig. 2. Isosurfaces of the radial component of the librating flow for $\mathcal{E} = 0.5$, $E = 10^{-4}, \hat{\omega} = 1.2$ and $Po = 0.3$: (a) from the explicit scheme and (b) from the implicit scheme. Isosurfaces of the latitudinal component of the flow for $\mathcal{E} = 0.5$, $E = 10^{-4}, \hat{\omega} = 1.2$ and $Po = 0.3$: (c) from the explicit scheme and (d) from the implicit scheme.

We shall focus on the fully discrete finite element method with the second order Crank-Nicolson scheme in this section. Both implicit and explicit versions are described. We refer to the finite element system (28) and (29) the implicit Crank-Nicolson scheme which is re-written below with detailed terms for the purpose of numerical implementation. The subscript h shall be dropped through out this section for simplicity.

$$
\begin{aligned}
&\int_V \left(\frac{\mathbf{u}^{n+1}-\mathbf{u}^n}{\tau}\right)\cdot\mathbf{v}\,\mathrm{d}V + \int_V E\nabla\frac{\mathbf{u}^{n+1}+\mathbf{u}^n}{2}\cdot\nabla\mathbf{v}\,\mathrm{d}V \\
&\quad+\frac{1}{2}\Big\{\int_V\left(\frac{3}{2}\mathbf{u}^n-\frac{1}{2}\mathbf{u}^{n-1}\right)\cdot\nabla\frac{\mathbf{u}^{n+1}+\mathbf{u}^n}{2}\cdot\mathbf{v}\,\mathrm{d}V \\
&\quad-\int_V\left(\frac{3}{2}\mathbf{u}^n-\frac{1}{2}\mathbf{u}^{n-1}\right)\cdot\nabla\mathbf{v}\cdot\frac{\mathbf{u}^{n+1}+\mathbf{u}^n}{2}\,\mathrm{d}V\Big\} \\
&\quad+\int_V 2\hat{\mathbf{z}}\times\frac{\mathbf{u}^{n+1}+\mathbf{u}^n}{2}\cdot\mathbf{v}\,\mathrm{d}V-\int_V\frac{p^{n+1}+p^n}{2}\nabla\cdot\mathbf{v}\,\mathrm{d}V \\
&\quad=\int_V 2Po\left[\hat{\omega}^{-1}\hat{\mathbf{y}}\times\frac{\mathbf{u}^{n+1}+\mathbf{u}^n}{2}\cos(\hat{\omega}t_{n+1/2})-\hat{\mathbf{x}}\times\frac{\mathbf{u}^{n+1}+\mathbf{u}^n}{2}\sin(\hat{\omega}t_{n+1/2})\right]\cdot\mathbf{v}\,\mathrm{d}V \\
&\quad+\int_V Po\Big[\hat{\omega}\mathbf{r}\times\hat{\mathbf{x}}\cos\left(\hat{\omega}t_{n+1/2}\right)+\mathbf{r}\times(\hat{\mathbf{z}}\times\hat{\mathbf{x}})\sin\left(\hat{\omega}t_{n+1/2}\right)\Big]\cdot\mathbf{v}\,\mathrm{d}V, \qquad (39)\\
&\quad-\int_V q\nabla\cdot\frac{\mathbf{u}^{n+1}+\mathbf{u}^n}{2}\,\mathrm{d}V=0, \qquad (40)
\end{aligned}
$$

where V denotes the triaxial ellipsoidal volume. Note the implicit non-linear term has been symmetrized (cf. Equation (12)). We also present an explicit Crank-Nicolson scheme in which the nonlinear term $\mathbf{u}\cdot\nabla\mathbf{u}$ at $t=t_{n+1/2}$ is expressed as

$$
\mathbf{u}^{n+1/2}\cdot\nabla\mathbf{u}^{n+1/2}=\frac{3}{2}(\mathbf{u}^n\cdot\nabla\mathbf{u}^n)-\frac{1}{2}(\mathbf{u}^{n-1}\cdot\nabla\mathbf{u}^{n-1})+O(\tau^2). \qquad (41)
$$

The explicit analogy of (39) and (40) is

$$\int_V \left(\frac{\mathbf{u}^{n+1}-\mathbf{u}^n}{\tau}\right)\cdot\mathbf{v}\,\mathrm{d}V + \int_V E\nabla\frac{\mathbf{u}^{n+1}+\mathbf{u}^n}{2}\cdot\nabla\mathbf{v}\,\mathrm{d}V$$
$$+\int_V\left[\frac{3}{2}(\mathbf{u}^n\cdot\nabla\mathbf{u}^n)-\frac{1}{2}(\mathbf{u}^{n-1}\cdot\nabla\mathbf{u}^{n-1})\right]\cdot\mathbf{v}\,\mathrm{d}V$$
$$+\int_V 2\hat{\mathbf{z}}\times\frac{\mathbf{u}^{n+1}+\mathbf{u}^n}{2}\cdot\mathbf{v}\,\mathrm{d}V-\int_V\frac{p^{n+1}+p^n}{2}\nabla\cdot\mathbf{v}\,\mathrm{d}V$$
$$=\int_V 2Po\left[\hat{\omega}^{-1}\hat{\mathbf{y}}\times\frac{\mathbf{u}^{n+1}+\mathbf{u}^n}{2}\cos(\hat{\omega}t_{n+1/2})-\hat{\mathbf{x}}\times\frac{\mathbf{u}^{n+1}+\mathbf{u}^n}{2}\sin(\hat{\omega}t_{n+1/2})\right]\cdot\mathbf{v}\,\mathrm{d}V$$
$$+\int_V Po\Big[\hat{\omega}\mathbf{r}\times\hat{\mathbf{x}}\cos\left(\hat{\omega}t_{n+1/2}\right)+\mathbf{r}\times(\hat{\mathbf{z}}\times\hat{\mathbf{x}})\sin\left(\hat{\omega}t_{n+1/2}\right)\Big]\cdot\mathbf{v}\,\mathrm{d}V, \tag{42}$$
$$-\int_V q\nabla\cdot\frac{\mathbf{u}^{n+1}+\mathbf{u}^n}{2}\,\mathrm{d}V=0. \tag{43}$$

It should be pointed out that, since the Coriolis term $\hat{\mathbf{z}}\times\mathbf{u}^{n+1}$ is primarily dominant, two other Coriolis terms in (39) and (42), $Po\hat{\omega}^{-1}\hat{\mathbf{y}}\times\mathbf{u}^{n+1}\cos(\hat{\omega}t_{n+1/2})$ and $Po\hat{\mathbf{x}}\times\mathbf{u}^{n+1}\sin(\hat{\omega}t_{n+1/2})$, are small and insignificant when $Po\ll 1$. There exist no noticeable differences between the numerical solutions obtained with or without having the two small Coriolis terms.

Mixed finite element of the Hood-Taylor type [9] is used in the numerical implementation. The pressure p^{n+1} is uniquely determined up to an additive constant. An additional condition $p^{n+1}(\mathbf{r}_0)=$ constant is imposed at a selected point $\mathbf{r}_0$ numerically. The equations of implicit and explicit Crank-Nicolson schemes are solved efficiently on modern parallel computers, starting from an arbitrary initial condition to find $\mathbf{u}^{n+1}$, p^{n+1} from given $\mathbf{u}^n$ and $\mathbf{u}^{n-1}$ together with the non-slip boundary condition.

5.3 Application and results

For the purpose of understanding the effect of different numerical schemes on simulating a nonlinear flow in librating triaxial ellipsoids, we have implemented the finite element method for two different codes based on the implicit and explicit Crank-Nicolson schemes. Starting from the same initial condition with exactly the same parameters of the problem, we have simulated various librating flows for testing two different numerical schemes.

Figure 1 shows the time-dependent kinetic energies, $E_{\mathrm{kin}}(t)$, defined as

$$E_{\mathrm{kin}}(t)=\frac{1}{2V}\int_V|\mathbf{u}(\mathbf{r},t)|^2\mathrm{d}V, \tag{44}$$

of the nonlinear librating flow as a function of time for $\mathcal{E}=0.5, Po=0.3$ at $E=10^{-4}$, where $\int_V$ denotes the integral over the triaxial ellipsoidal cavity. Two different numerical solutions are displayed in the figure: the solid line

is obtained from the implicit Crank-Nicolson scheme while the dashed line from the explicit Crank-Nicolson scheme. Evidently, there are no noticeable differences between the two different solutions that are obtained using different numerical schemes. Figure 2 shows the spatial structure of the librating flows from the two different solutions. It again reveals that there exist no substantial differences between the implicit and explicit second-order schemes.

It is important to note, however, that the current numerical simulation is limited to a weakly nonlinear regime of the parameter space. In other words, the nonlinear effect is not predominant in these nonlinear numerical solutions. We cannot exclude the possibility that the librationally resonant flow at very small Ekman number E and sufficiently large Po requires the implicit Crank-Nicolson scheme in order to accurately capture the nonlinear effect of the numerical solution.

6 SUMMARY AND REMARKS

As a result of rapid rotation and interaction between planets and stars, many planetary bodies are in the shape of a triaxial ellipsoid. This paper presents the theoretical analysis for a finite element method that can be used to compute nonlinear time-dependent librating flows confined in librating triaxial ellipsoidal cavities with arbitrary eccentricity $0 \leq \mathcal{E} < 1$, providing a mathematical foundation for the geophysical and astrophysical application of the numerical method.

In comparison to the spectral method, the finite element method is based on the three-dimensional triangulation of a triaxial ellipsoidal domain with the velocity and pressure being represented by continuous piecewise quadratic and linear finite elements. We have discussed the stability properties of the finite element solution and estimated the numerical errors of the finite element approximation. Additionally, we have implemented two different temporal schemes with the same spatial tetrahedral discretization for simulating fluid motion in a librating triaxial ellipsoid. To authors' best knowledge, this paper represents the first theoretical study on a finite element scheme for simulating a nonlinear librating flow in triaxial ellipsoidal geometry.

The numerical scheme presented in this paper would be also suitable for simulating dynamo action taking place in nearly synchronous planets and moons that are thermally or chemically non-convective. Although it is widely accepted that thermal or chemical buoyancy within planetary fluid cores drive their dynamos, exceptional cases exist for certain planets, such as Mercury and Ganymede, which may require an alternative mechanism of sustaining their dynamos. But the extension of a similar theoretical study to include

both the effect of the magnetic field on the flow and the dynamo equation [23] in a librating triaxial ellipsoid is highly challenging and will be addressed in a future paper.

Acknowledgements

K. H. C. is supported by Hong Kong RGC grant/700310, Y. H. is supported by the NSF of China grant 10971166, K. Z. is supported by U.K. NERC, Royal Society, Leverhulme grants and J. Z. is supported by Hong Kong RGC grants 405110 and 404611. Part of this work (K. Z.) was carried out at, and supported by, the Institute of Mathematical Sciences, the Chinese University of Hong Kong.

References

[1] K. Chan, K. Zhang, J. Zou, Spherical interface dynamos: mathematical theory, finite element approximation, and application, SIAM J. Numerical Analysis 44 (2006) 1877–1902.

[2] K. Chan, K. Zhang, L. Li, X. Liao, A new generation of convection-driven spherical dynamos using EBE finite element method, Physics of the Earth and Planetary Interiors 163 (2007) 251–265.

[3] Z. Chen, J. Zou, Finite element methods and their convergence for elliptic and parabolic interface problems, Numerische Mathematik 79 (1998) 175–202.

[4] P.G. Ciarlet, The Finite Element Method for Elliptic Problems, first ed., North-Holland Pub. Co., Amsterdam/New York, 1978.

[5] M.E. Everett, A three-dimensional spherical mesh generator, Geophysical Journal International 130 (1997) 193–200.

[6] M. Feistauer, A. Zenisek, Finite element solution of nonlinear elliptic problems, Numerische Mathematik 50 (1987) 451–475.

[7] V. Girault, P. Raviart, Finite Element Approximation of the Navier-Stokes Equations, Springer: New York, 1981.

[8] V. Girault, P. Raviart, Finite Element Methods for Navier-Stokes Equations: Theory and Algorithms, Springer: Berlin, 1986.

[9] P. Hood, C. Taylor, Navier-Stokes equations using mixed-interpolation. In *Finite Element Methods in Flow Problems*, J.T. Oden, O.C. Zienkiewicz, R.H. Gallagher, C. Taylor (eds). UAH Press: Huntsville, 1974; 57–66.

[10] Y.N. He, Fully discrete stabilized finite element method for the time-dependent Navier-Stokes equations, IMA J. Numer. Anal. 23 (2003) 1–27.

[11] Y.N. He, The Euler implicit/explicit scheme for the 2D time-dependent Navier-Stokes equations with smooth or non-smooth initial data, Math. Comp., 77 (2008) 2097–2124.

[12] J.G. Heywood, R. Rannacher, Finite element approximation of the nonstationary Navier-Stokes problem I: Regularity of solutions and second-order error estimates for spatial discretization, SIAM J. Numer. Anal., 19 (1982) 275–311.

[13] J.G. Heywood, R. Rannacher, Finite element approximation of the nonstationary Navier-Stokes problem III: Smoothing property and high order error estimates for spatial discretization, SIAM J. Numer. Anal., 25 (1988) 489–512.

[14] J.G. Heywood, R. Rannacher, Finite element approximation of the nonstationary Navier-Stokes problem IV: Error Analysis for second-order time discretization, SIAM J. Numer. Anal., 27 (1990) 353–384.

[15] H. Johnston, J.G. Liu, Accurate, stable and efficient Navier-Stokes solvers based on explicit treatment of the pressure term, J. Computational Physics, 199 (2004) 221–259.

[16] D. Kong, K. Zhang, G. Schubert, Shapes of two-layer models of rotating planets, Journal of Geophysical Research 115 (2010) E12003.

[17] S. Lorenzani, A. Tilgner, Fluid instabilities in precessing spheroidal cavities, Journal of Fluid Mechanics 447 (2001) 111–128.

[18] J.L. Margot, S.J. Peale, R.F. Jurgens, M.A. Slade, I.V. Holin, Large longitude libration of mercury reveals a molten core, Science 316 (2007) 710–714.

[19] M. Marion, R. Temam, Navier-Stokes equations: Theory and approximation, in: Handbook of Numerical Analysis, Vol. VI, 503–688, North-Holland, Amsterdam, 1998.

[20] D. Schmitt, Numerical study of viscous modes in a rotating spheroid, Journal of Fluid Mechanics 567 (2006) 399–414.

[21] F. Tone, Error analysis for a second order scheme for the Navier-Stokes equations, Applied Numerical Mathematics, 50 (2004) 93–119.

[22] O.C. Zienkiewicz, The finite element method, third ed., McGraw-Hill: London, 1977.

[23] K. Zhang, K. Chan, J. Zou, X. Liao, G. Schubert, A three-dimensional spherical nonlinear interface dynamo, Astrophysical Journal 596 (2003) 663–679.

[24] K. Zhang, K. Chan, X. Liao, Asymptotic theory of resonant flow in a spheroidal cavity driven by latitudinal libration, Journal of Fluid Mechanics 692 (2012) 420–445.